Available online at www.sciencedirect.com
SCIENCE DIRECT
Journal of Catalysis 227 (2004) 270–281
JOURNAL OF CATALYSIS
www.elsevier.com/locate/jcat

Surface species during the crystallization of $VOHPO_4 \cdot 0.5H_2O$

Leonard O'Mahony, Teresa Curtin, Dmitry Zemlyanov *, Miroslav Mihov, B. Kieran Hodnett

Materials and Surface Science Institute, University of Limerick, Limerick, Ireland

Received 26 April 2004; revised 22 June 2004; accepted 24 June 2004

Available online 24 August 2004

Abstract

The synthesis of $VOHPO_4 \cdot 0.5H_2O$ by reaction of a reduced suspension/solution of V_2O_5 in alcohol and *o*-H_3PO_4 has been studied by in situ X-ray diffraction (XRD) and ex situ X-ray photoelectron spectroscopy (XPS) and focused ion beam (FIB) microscopy, including cross-sectioning. XPS, XRD, and microscopy evidence is presented for the temporal dissolution of V_2O_5 and formation of $VOPO_4 \cdot 2H_2O$, $VOPO_4 \cdot H_2O$, and $VOHPO_4 \cdot 0.5H_2O$. The XPS technique allows us to trace the development of surface vanadium, oxygen, and carbon states as well as the surface P:V ratio. Four vanadium species were identified. The oxygen vacancies on the surface were characterised by the V $2p_{3/2}$ peak at 515.5 eV and by the O 1s peak at 531.2 eV. V_2O_5 exhibited the V $2p_{3/2}$ peak at 517.4 eV and the O 1s peak at 530.0 eV. The dihydrate phase $VOPO_4 \cdot 2H_2O$ and hydrate phase $VOPO_4 \cdot H_2O$ were monitored by the V $2p_{3/2}$ peak at 518.1 eV and the O 1s peak at 531.2 eV. The VPO catalyst precursor $VOHPO_4 \cdot 0.5H_2O$, the V^{4+} oxidation state, shows the V $2p_{3/2}$ peak at 516.6 eV and the O 1s peak at 531.2 eV. The O 1s peak at 532.9 eV is assigned to crystal water. In situ monitoring of the synthesis by XRD was in a good agreement with the ex situ XPS analysis. $VOPO_4 \cdot 2H_2O$ and $VOPO_4 \cdot H_2O$ were successfully identified by XPS as a metastable phase, which forms at short synthesis times. As the hydrate phase concentration decreases the concentration of $VOHPO_4 \cdot 0.5H_2O$ increases. All XPS data were consistent with the earlier proposed mechanism, which supposed that $VOPO_4 \cdot 2H_2O$ dehydrates to $VOPO_4 \cdot H_2O$, delaminates and the delaminated edges of $VOPO_4 \cdot H_2O$ serve as the nucleation point for growth of $VOHPO_4 \cdot 0.5H_2O$.

Keywords: Crystal morphology; Nucleation; Vanadium phosporus oxide catalyst; XPS; In situ XRD; Surfaces; Growth from solutions; Phosphates; Vanadates

1. Introduction

The vanadium phosphorus oxide catalyst is commercially applied for the selective oxidation of *n*-butane to maleic anhydride [1]. Several V(IV) and V(V) phosphate phases exist in the VPO system and the correlation of catalytic performance with crystalline structure has been reviewed [2–4].

Among all these phases, $VOHPO_4 \cdot 0.5H_2O$ is particularly important since it is the precursor of the $(VO)_2P_2O_7$ phase observed in the final activated catalyst [1]. The active VPO catalyst presents a twisted platelet habit of varying crystallinity and features small amounts of V^{5+} phases, most notably α-$VOPO_4$ [5,6]. The active site for *n*-butane oxidation to maleic anhydride has been proposed as being the (200) plane of vanadyl pyrophosphate [3,7–11]. Evidence has been presented that the yield of maleic anhydride improves when the exposure of the (200) plane of $(VO)_2P_2O_7$ is maximised [11], leading to the proposal that the active site for *n*-butane activation and oxyfunctionalisation resides on this plane [12]. Some argue that the V^{5+}/V^{4+} species in the topmost oxidised layer of vanadyl pyrophosphate are the active sites [13], while others believe that the active sites lie within the microdomains of crystalline vanadyl (V^{5+}) orthophosphates, formed as the (200) faces of vanadyl pyrophosphate under catalytic reaction conditions [2].

Despite the fact that the preparation of high activity catalysts has been a major theme for a number of investigations [6,11,14,15], the origin of the $(VO)_2P_2O_7$ morphology has not been established. Many features of the final catalyst, such as crystalline habit and particle size, are established

* Corresponding author. Fax: 353 (0)61 213529.
E-mail address: dima.zemlianov@ul.ie (D. Zemlyanov).

0021-9517/$ – see front matter
doi:10.1016/j.jcat.2004.06.020

when the precursor forms [2,16]. Hence, the synthesis route and reaction conditions during synthesis affect the morphology of $VOHPO_4 \cdot 0.5H_2O$ and ultimately the catalyst performance [1,17,18]. Consequently careful preparation of the precursor $VOHPO_4 \cdot 0.5H_2O$ is the key to obtaining an effective catalyst [4,8].

A tentative crystallisation mechanism of $VOHPO_4 \cdot 0.5H_2O$ in organic media was proposed by O'Mahony et al. [19], in which $VOPO_4 \cdot 2H_2O$ forms rapidly when *ortho*-H_3PO_4 is added to a refluxing mixture of V_2O_5 in alcohol. This phase converts to $VOPO_4 \cdot H_2O$, which in turn acts as the nucleation point from which the $VOHPO_4 \cdot 0.5H_2O$ phase grows epitaxially into the familiar rosette-like habit. In this paper, the proposed mechanism was examined by following the synthesis of $VOHPO_4 \cdot 0.5H_2O$ in situ by energy-dispersive X-ray diffraction (XRD) and ex situ by X-ray photoelectron spectroscopy (XPS) and focused ion beam (FIB) microscopy. There are a number of reported XPS studies of fully formed VPO catalysts [20–26], but in this paper the XPS technique was applied to samples taken from a refluxing *ortho*-H_3PO_4/V_2O_5/alcohol mixture for synthesis times in the range 0.5–120 min to gain insight into the nature of the surface species present during crystallisation of $VOHPO_4 \cdot 0.5H_2O$.

2. Experimental

A typical protocol of the VPO precursor preparation consists of refluxing V_2O_5 (Merck) in a 90:10 mixture of 2-methylpropan-1-ol (BDH Analar) and benzyl alcohol (Riedel–de Haen) for 4 h at a reflux temperature of 108 °C. An 85% *ortho*-phosphoric acid (Aldrich) solution was then added to the resulting vanadium suspension and was refluxed for a further 2 h. The reactant P:V mole ratio was 1:1. For the ex situ analysis, VPO samples were recovered at times from 0.5 to 120 min following phosphorus (o-H_3PO_4) addition. Below in this publication, this time is refereed to as the synthesis time. The recovered solids were filtered and dried at 120 °C.

A focused ion beam microscope FEI 200 was used to obtain precursor images. Samples were coated with gold in an EMITECH K550 sputter coater. The focus ion beam system is similar to the SEM, the major difference being the use of a gallium ion (Ga^+) beam instead of an electron beam. The beam energy is typically 30 keV, with a beam current in the range of 1 to 11500 pA. As the beam strikes the sample, secondary electrons and secondary ions are emitted from the sample surface. Secondary electrons are generated in much greater quantities than ions and provide images of better quality and resolution. Cross-section analyses of VPO precursor particles were performed by applying a high current beam (350–1000 pA). For typical cross-section analysis, a crater (15–20 μm in diameter) was milled in the sample and imaging was performed on the original vertical wall of the crater after tilting at 45°.

In preparation for in situ diffraction studies, V_2O_5 (Merck) was refluxed in a 90:10 mixture of 2-methylpropan-1-ol (BDH Analar) and benzyl alcohol (Riedel–de Haen) for 4 h. 85% H_3PO_4 (P:V = 1:1) was added to this prepared suspension in a Teflon-lined stainless-steel cell under constant stirring. The temperature of the sample under study was automatically controlled and measured using a thermocouple directly inserted into the sample cell. The evolution of crystalline phases with time was then recorded in situ, using the energy-dispersive X-ray diffraction setup at Station 16.4 of the U.K. Synchrotron Radiation Source (SRS) at the CLRC Daresbury Laboratory, UK. The SRS is a low emittance storage ring, which runs with an electron beam energy of 2 GeV. The ring current was approximately 180–250 mA during experiments. Station 16.4 is a white beam facility, where a wiggler magnet of peak field 6 T is located. Rather than using conventional monochromatic radiation with an angle-scanning detector, the energy-dispersive method uses a continuum source of X-ray wavelengths with an energy-dispersive detector fixed at a chosen angle (2θ). The ED detector differentiates X-ray photons according to their particular energies E and resolutions $\Delta E/E$ typically of a few percent are achieved. This technique generates diffraction patterns in E rather than 2θ with all patterns being converted to d-spacing values in this presentation [27–29]. This system utilises a multidetector system, which collects XRD patterns from a sample simultaneously at different angles. Two detectors are used, each with a separate postsample collimator and Germanium crystal detector. The set positions record patterns in the regions of 2–5 and 4–15 Å, respectively. A time delay of 10–15 min has been observed during the experiment for the sample cell to come up to temperature and therefore must be considered when diffraction data are observed.

XPS data were obtained by a Kratos AXIS 165 spectrometer using monochromatic Al-K_α radiation ($h\nu$ = 1486.58 eV) and fixed analyser pass energy of 20 eV. The atomic concentrations of the chemical elements in the near-surface region were estimated after the subtraction of a Shirley-type background [30], taking into account the corresponding Scofield atomic sensitivity factors [31]. The binding energy (BE) values referred to the Fermi level were calibrated using the C 1s 284.80 eV, the standard deviation of the peak position associated with the calibration procedure was ±0.05 eV. A commercial Kratos charge neutraliser was used to achieve a resolution of 0.9 eV measured as a full width at half-maximum (FWHM) of the V 2p deconvoluted peaks. The XPS spectra were fitted by CasaXPS software assuming line shape to be a product of Doniach–Sunjic and Gaussian–Lorentzian functions [32,33].

3. Results

Refluxing V_2O_5 in a 90:10 2-methylpropan-1-ol:benzyl alcohol mixture for 4 h leads to the dissolution of ca. 30–40% of the available vanadium oxide. Fig. 1 presents the in situ diffraction patterns of the VPO phases that develop when phosphoric acid was added to the vanadium oxide solution/suspension. The reactant P:V mole ratio was 1:1. The (010), (101), and (310) reflections of V_2O_5 decrease in intensity with time of synthesis and completely disappears after 24–28 min as demonstrated by the XRD patterns in the left panel of Fig. 1. By this time the reflection characteristics of $VOHPO_4 \cdot 0.5H_2O$ namely (101), (021), (121), (201), and (220) begin to form. Crystallisation of hemihydrate precursor was followed by plotting the integrated areas of the respective peaks as shown in the right panel of Fig. 1. The areas were determined by fitting the individual peaks assuming a Gaussian line-shape. Another consistent feature of this data is the emergence of a peak at 3.1 Å, hardly present at 2 min, but a major feature in the diffraction pattern after 4 min. This feature was consistently present until approximately 30 min and regains intensity as the hemihydrate formed fully, at which point was indexed as the (201) plane of $VOHPO_4 \cdot 0.5H_2O$. In Ref. [19] the peak at 3.1 Å was assigned to the (200) reflection of vanadyl phosphate hydrate ($VOPO_4 \cdot H_2O$) or vanadyl phosphate dihydrate ($VOPO_4 \cdot 2H_2O$). This assignment is consistent with the appearance of the hydrate phases, which was also monitored by a reflection at $d = 6.7$–7.5 Å (the XRD patterns not shown here) [19]. This reflection appeared at 7.5 Å at 4-min synthesis time and shifted gradually to 6.7 Å after 24–28 min. These features were identified as $VOPO_4 \cdot 2H_2O$ ($d_{001} = 7.45$ Å), which converts to $VOPO_4 \cdot H_2O$ ($d_{001} = 6.37$ Å) [19].

Fig. 2 presents the FIB micrographs of VPO sample recovered after 0.5-min synthesis time. Unreacted V_2O_5 can normally be observed in micrographs of materials isolated at this time. Thin platelets of dimension $10 \times 10 \times 0.2$ μm can be seen. Some platelets appear to have cracks in their uppermost layers and have delaminated. EDX analy-

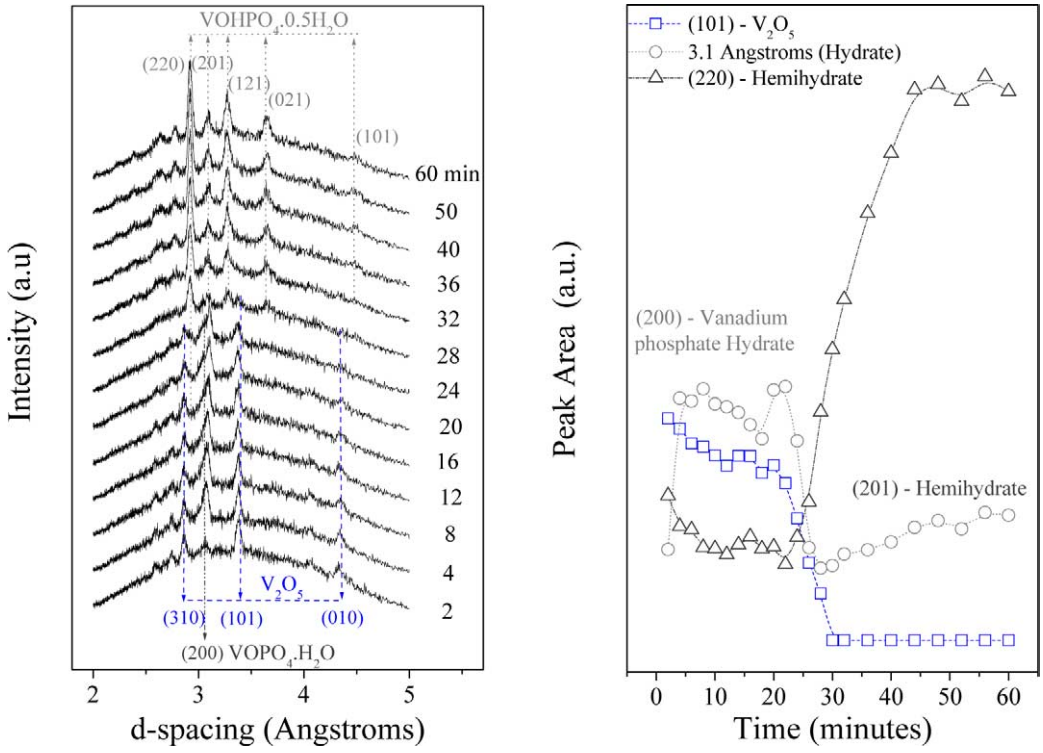

Fig. 1. In situ energy dispersive XRD patterns of $VOHPO_4 \cdot 0.5H_2O$ evolution from V_2O_5 at 108 °C with a reactant P:V molar ratio of 1:1. Crystallisation of hemihydrate precursor was followed by plotting the integrated intensities of the respective peaks.

Table 1
V 2p core-level characteristics of vanadium oxidation states

Assignment	Oxidation state	V $2p_{1/2}$ peak		V $2p_{3/2}$ peak	
		BE (eV)	FWHM (eV)	BE (eV)	FWHM (eV)
Oxygen defect of V_2O_5	V^{3+}	522.80 ± 0.15	1.20 ± 0.20	515.50 ± 0.15	1.30 ± 0.05
$VOHPO_4 \cdot 0.5H_2O$	V^{4+}	523.85 ± 0.15	1.90 ± 0.10	516.55 ± 0.15	1.20 ± 0.10
V_2O_5	V^{5+}	524.65 ± 0.10	1.60 ± 0.30	517.35 ± 0.10	1.00 ± 0.05
$VOPO_4 \cdot 2H_2O$ and/or $VOPO_4 \cdot H_2O$	V^{5+}	525.45 ± 0.05	1.2 ± 0.20	518.10 ± 0.05	1.00 ± 0.10

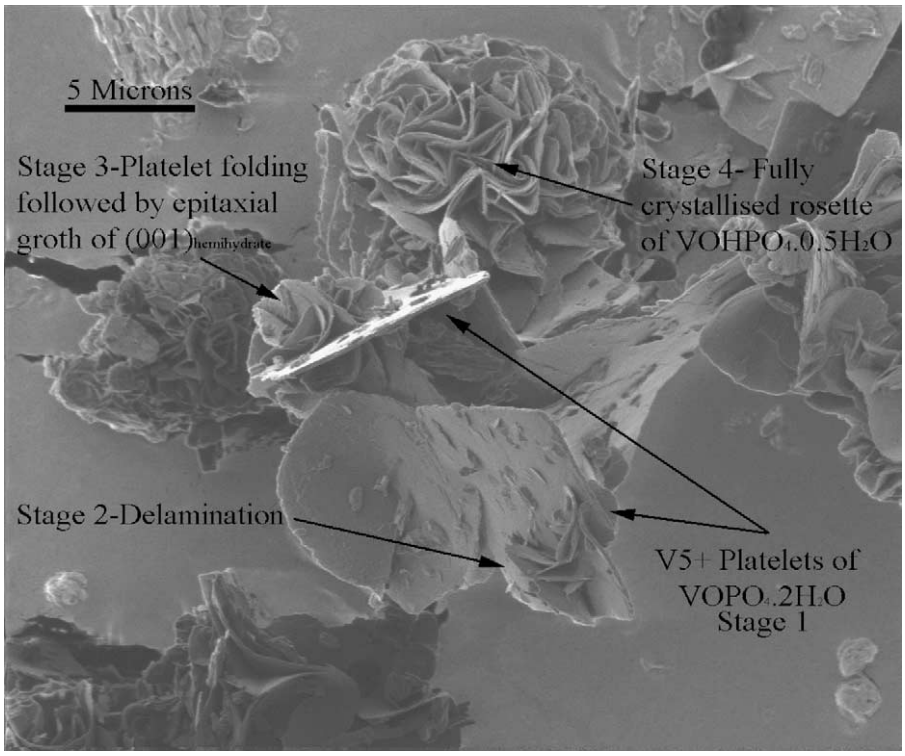

(a)

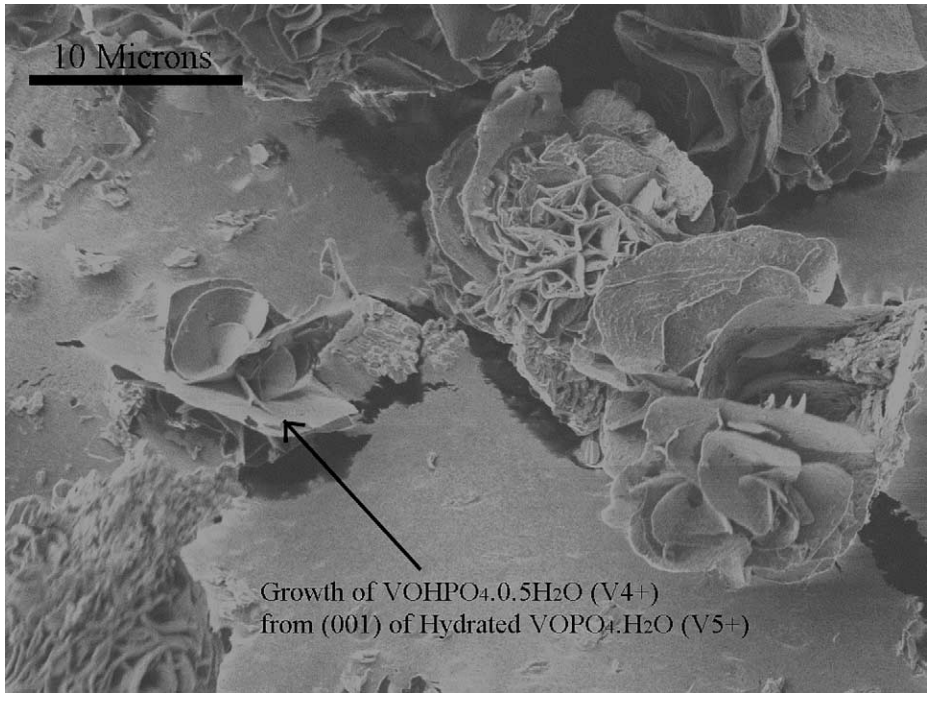

(b)

Fig. 2. (a and b) FIB images of VPO sample recovered after 0.5-min synthesis. Points of consideration: 10 × 10-μm platelets are representative of a hydrated vanadyl phosphate phase, V^{5+}. Note: Platelet delamination and distortion observed here.

sis of the platelets indicating the presence of phosphorus and vanadium and these platelets never appeared prior to the addition of *ortho*-H_3PO_4. The platelets are attributed to $VOPO_4 \cdot 2H_2O$ and they delaminate as they transform into $VOPO_4 \cdot H_2O$. This transformation corresponds to a d-spacing shift from d_{001} $VOPO_4 \cdot 2H_2O = 7.5$ Å to d_{001} $VOPO_4 \cdot H_2O = 6.7$ Å. The formation of rosette-type particles is also noticeable. These rosette particles appear to have grown out of a now badly fragmented platelet as can be seen in Figs. 2a and 2b. The rosette morphology has been

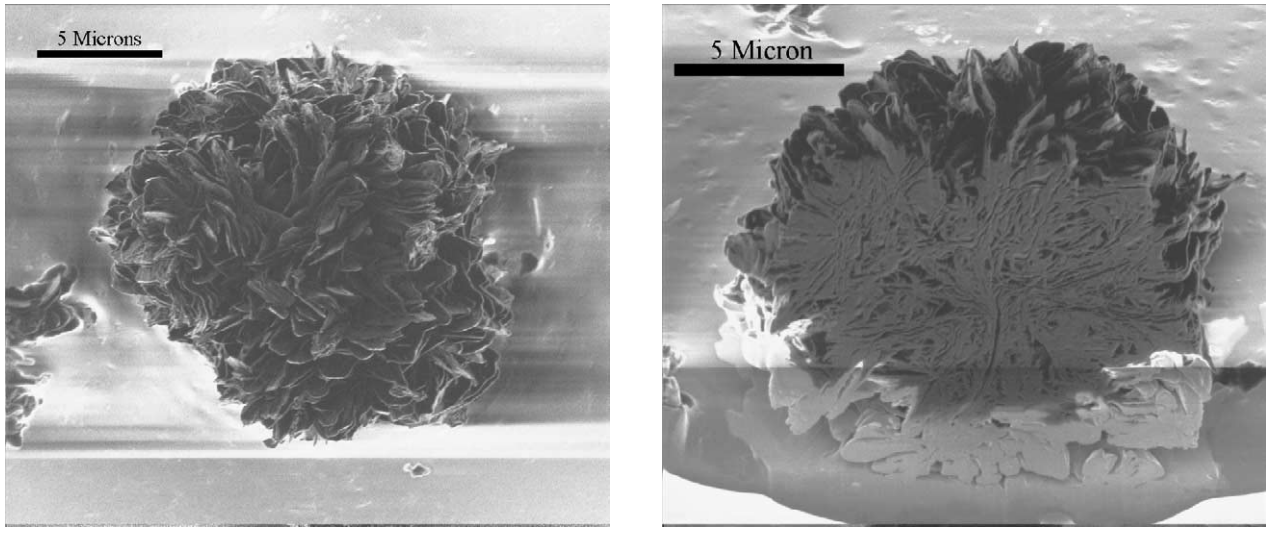

Fig. 3. (a) Rosette crystal recovered after 60 min of synthesis and (b) FIB cross section of this rosette crystal.

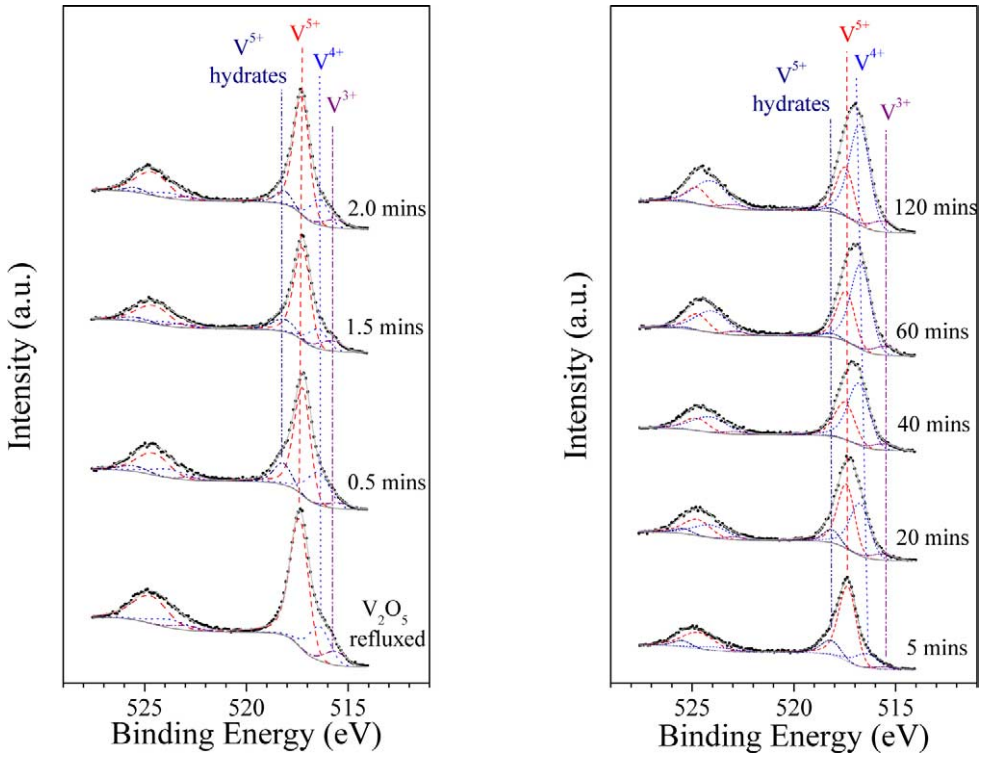

Fig. 4. V 2p core-level spectra obtained from VPO samples recovered after specified time. The bottom spectrum in the left panel characterises V_2O_5 refluxed in alcohol for 4 h. The "raw" experimental data are plotted as dots.

identified as the hemihydrate precursor phase, $VOHPO_4 \cdot 0.5H_2O$ [3,9], and is consistent with XRD data. An important point, which supports the proposed mechanism, is that $VOHPO_4 \cdot 0.5H_2O$ can be synthesised from $VOPO_4 \cdot 2H_2O$ [34]. After 60-min synthesis time (Fig. 3), the appearance of the $VOHPO_4 \cdot 0.5H_2O$ changes, and the FIB cross section confirms that a much denser interior to each particle is generated, indicating that the growth of $VOHPO_4 \cdot 0.5H_2O$ continues long after all the $VOPO_4 \cdot H_2O$ has been consumed. Typical platelet volumes taken from Fig. 2 ($10 \times 10 \times 0.2$ μm) are 20 μm^3 whereas typical particle volume (based on spherical with radius 6–7 μm) taken from Fig. 3 are 900–1400 μm^3.

A series of VPO precursors were prepared for XPS analysis. Fig. 4 presents the V 2p core-level spectra of the precursor evolving throughout the transformation process from V_2O_5 to $VOHPO_4 \cdot 0.5H_2O$. All the V $2p_{3/2}$ peaks are centered at approximately 517.4 eV but have a highly asymmetric shape with high and/or low BE shoulders that points

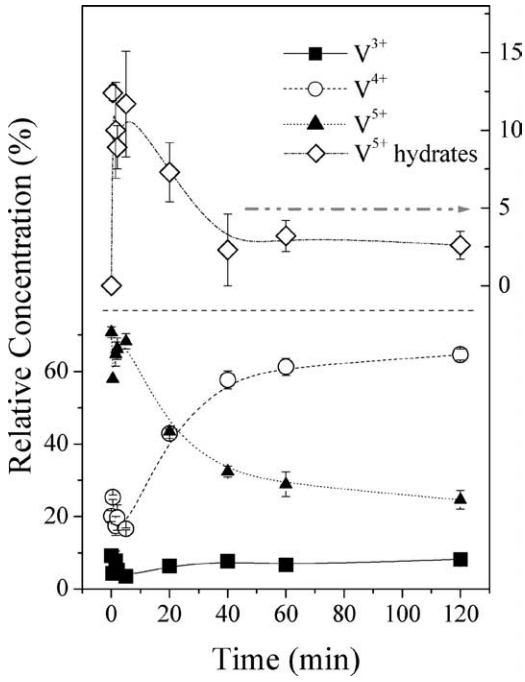

Fig. 5. Relative concentration of vanadium species by XPS as a function of the synthesis time.

to a multicomponent nature of the V 2p peaks. The V 2p peaks were fitted with four components assuming line shape to be a product of Doniach–Sunjic and Gaussian–Lorentzian functions [32,33]. The line shape was chosen with respect to the best fitting for monochromatic Al-K_α radiation [33]. The relative ratio and the split of the V 2p doublet were fixed during the fitting, whereas other parameters such as intensity, FWHM, and peak position were allowed to be varied within reasonable ranges. The four components denoted as V^{3+}, V^{4+}, V^{5+} and V^{5+} *hydrate* were distinguished. Their XPS characteristics are summarized in Table 1. Since the V $2p_{3/2}$ peak is much narrower than the V $2p_{1/2}$ peak, below we will focus our discussion mainly on the V $2p_{3/2}$ peak.

The relative concentration of the vanadium states is plotted in Fig. 5. The V^{3+} state was assigned to oxygen vacancies that appear on the surface of V_2O_5 during refluxing or in vacuum. Since the relative concentration of this state does not vary with synthesis time and is below 10%, this species will not be discussed with regard to the reaction mechanism. The main point of interest is the evolution of the V^{4+}, V^{5+}, and V^{5+} hydrate states, which are assigned to $VOHPO_4 \cdot 0.5H_2O$, V_2O_5, and $VOPO_4 \cdot H_2O/VOPO_4 \cdot 2H_2O$, respectively. At this stage the XPS data are consistent with in situ XRD observations. Thus, the (220) reflection of $VOHPO_4 \cdot 0.5H_2O$ grows with the synthesis time as shown in the right panel of Fig. 1. Consistently, the V $2p_{3/2}$ peak at 516.6 eV attributed to $VOHPO_4 \cdot 0.5H_2O$ gradually increases in intensity as well. Decrease of the diffraction peaks of V_2O_5 is in agreement with depleting the V 2p core level peak at 517.4 eV attributed to V_2O_5.

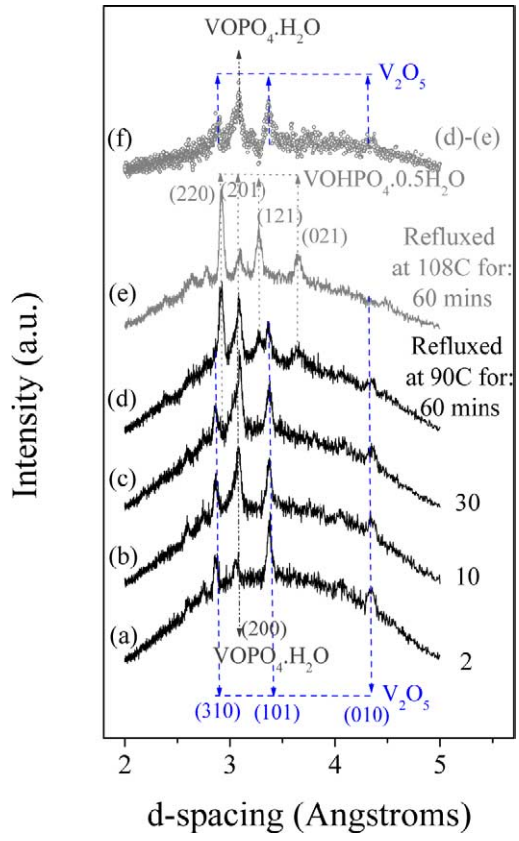

Fig. 6. In situ XRD of the V_2O_5 refluxed in alcohol and then refluxed (a–d) at 90 °C in the presence of an 85% *ortho*-phosphoric acid for the specified time, (e) at 108 °C for 60 min. Trace (f) was obtained by subtracting trace (e) from trace (d).

The assignment of the V 2p peak component at 518.1 eV to the hydrate phase ($VOPO_4 \cdot 2H_2O$ and/or $VOPO_4 \cdot H_2O$) deserves a special discussion. The hydrate phase ($VOPO_4 \cdot 2H_2O$ and $VOPO_4 \cdot H_2O$) was identified by the XRD peaks at 3.1 and 6.7–7.5 Å. The high BE shoulder of the V $2p_{3/2}$ peak at 518.1 eV, which is particularly well seen at 5-min synthesis time, was attributed to the hydrate phase. In order to prove this assignment, the sample with a high percentage of the hydrate phase was prepared as follows. V_2O_5 was refluxed in a 90:10 alcohol mixture of 2-methylpropan-1-ol and benzyl alcohol for 4 h at a temperature of 108 °C, which is the usual refluxing protocol. An 85% *ortho*-phosphoric acid solution was then added to the resulting vanadium suspension and further refluxed for 1 h at 90 °C (usually at 108 °C). The preparation of the hydrate-rich phase was monitored by in situ XRD as shown in Fig. 6. The VPO sample prepared through this protocol shows the intensive diffraction peak, at $d = 3.1$ Å associated with the hydrate phase. For sake of clarity, the difference between the diffraction patterns from the hydrate-rich phase and the hemihydrate phase is plotted in Fig. 6f. The "differential" pattern shows only the XRD peaks from unreacted V_2O_5 and $VOPO_4 \cdot H_2O$. XPS demonstrates that this sample is also characterised by the intensive V 2p component at 518.1 eV as shown in the left panel in Fig. 7 (trace c). This component is absent in

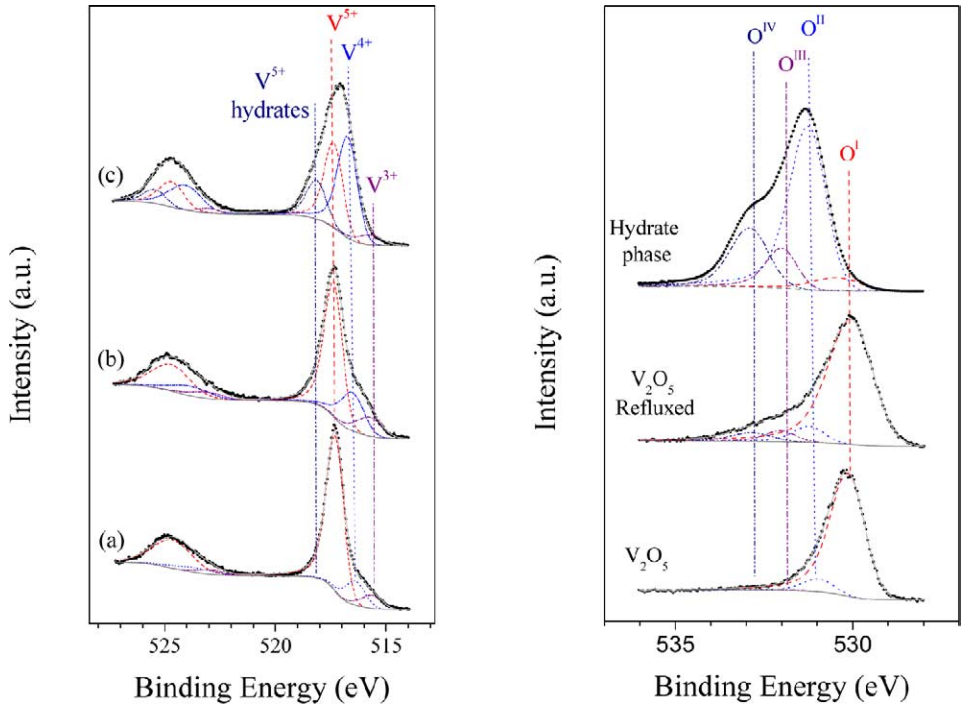

Fig. 7. The V 2p and O 1s core-level spectra obtained from (a) commercial V_2O_5 as received, (b) V_2O_5 refluxed in a 90:10 mixture of 2-methylpropan-1-ol and benzyl alcohol for 4 h at 108 °C, and (c) V_2O_5 refluxed as in (b) and then refluxed in the presence of 85% *ortho*-phosphoric acid for 1 h at 90 °C (the reactant P:V mole ratio was 1:1).

Table 2
XPS characteristic of the oxygen species

Oxygen species	Assignment	Nature	O 1s	
			BE (eV)	FWHM (eV)
O^I	Oxide-type oxygen, "ionic" bond	Oxygen defect of V_2O_5, V_2O_5 bulk	530.00 ± 0.10	1.30 ± 0.15
O^{II}	Phosphate, "covalent" bond	$VOPO_4 \cdot 2H_2O$, $VOPO_4 \cdot H_2O$ $VOHPO_4 \cdot 0.5H_2O$	531.15 ± 0.15	1.20 ± 0.15
O^{III}	OH groups	Hemihydrate phase, alcohol cracks	531.90 ± 0.15	1.10 ± 0.15
O^{IV}	H_2O	Crystal water in hydrate and hemihydrate phases, adsorbed water	532.90 ± 0.20	1.35 ± 0.25

the V 2p peaks obtained from commercial *as-received* V_2O_5 and vanadium oxide refluxed in the alcohol mixture (the left panel in Fig. 7 trace a and b, respectively). The V_2O_5 samples demonstrate only the three oxidation states named above as V^{3+}, V^{4+}, and V^{5+}. It is reasonable to suppose that refluxing in the alcohol mixture results in the reduction of vanadium; so the concentration of the V^{4+} state increases. On the other hand, the concentration of the V^{3+} state is approximately constant for all the samples; this also confirms the earlier assignment of the V^{3+} state to oxygen defects on the V_2O_5 surface, which does not necessarily form in the reaction with alcohols. Summarising the results of the XPS analysis one can unambiguously assign the V $2p_{3/2}$ component at 518.1 eV to the hydrates: $VOPO_4 \cdot 2H_2O$ and/or $VOPO_4 \cdot H_2O$.

The change in the vanadium oxidation states should also lead to changes in the oxygen states. Indeed, the hydrate-rich sample demonstrates a different shape and peak position for the O 1s line in comparison with the V_2O_5 samples as shown in the right panel in Fig. 7. Following the fitting procedure developed for the V 2p lines, the O 1s peaks were fitted with four components assuming line shape to be a product of Doniach–Sunjic and Gaussian–Lorentzian functions [32,33]. The major component of the O 1s line obtained from vanadium oxide is a peak at 530.0 eV denoted as an O^I state. This oxygen species is identified as oxide-type oxygen. The oxide oxygen is also the main component of the O 1s peak for the refluxed V_2O_5 sample, which shows an additional high BE shoulder fitted by two components at 531.9 and 532.9 eV denoted as O^{III} and O^{IV} states. These oxy-

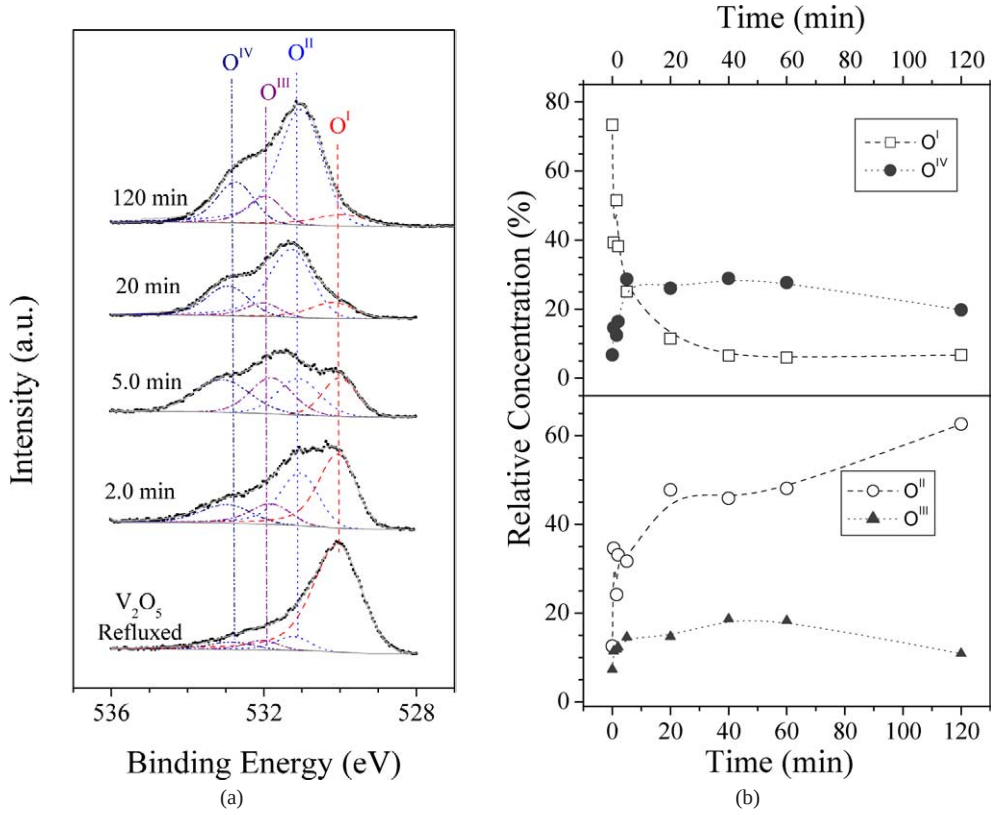

Fig. 8. a) O 1s core level spectra obtained from VPO samples recovered after specified time. The bottom spectrum characterises V_2O_5 refluxed in alcohol for 4 h. (b) Relative concentration of the oxygen species as a function of the synthesis time.

gen states were tentatively attributed to hydroxyl groups and crystallite water, respectively. A peak at 531.2 eV (O^{II} state) is the main feature of the hydrate-rich sample and therefore this peak could be assigned to phosphate-type oxygen. The XPS characteristics of the oxygen species are summarised in Table 2.

As shown in Fig. 5, the concentration of the hydrate phase monitored by XPS passes a maximum at 5-min synthesis time and then falls down almost to zero. It is noteworthy that a similar behaviour was monitored by XRD: the diffraction reflection of the hydrate phase at 3.1 Å (Fig. 1) and 6.7–7.5 Å [19] also passes through a maximum and then disappears.

The transformation of oxygen and carbon chemical states was monitored by XPS as well: Figs. 8 and 9 show the O 1s and C 1s core-level spectra, respectively, obtained from the VPO samples described in Fig. 4. The depleting of the ionic oxygen peak (O^I state) reflects the consumption of V_2O_5 in the reaction, whereas the growth of the peak at 531.2 eV corresponds to the formation of phosphate species such as $VOPO_4 \cdot 2H_2O$, $VOPO_4 \cdot H_2O$, or $VOHPO_4 \cdot 0.5H_2O$. The concentration of hydroxyl groups traced by the component at 532 eV (O^{III}) increases at an early stage of synthesis and after 5 min remains approximately constant. The amount of water (O^{IV}) also increases during the first 5 min and then decreases slightly.

Carbon species mainly exists in two chemical states represented by peaks at 284.8 and 286.3 eV; the peaks are attributed to hydrocarbons and to partially oxidised hydrocarbons, respectively. Carbonyls associated with the barely distinguishable component at 288.5 eV do not contribute much. Their relative concentration is below 5% and it does not change during the reaction. In general, the carbon percentage in the VPO samples decreases with the synthesis time, whereas the amount of partially oxidised hydrocarbon increases. It is remarkable that refluxing V_2O_5 in alcohols results in a slight increase of oxidised hydrocarbon, but their concentration grows faster in an acidic media.

The P:V ratio is an issue widely discussed in the literature [1]. The P:V ratio was calculated from the XPS data of the VPO samples recovered after different synthesis times as shown in Fig. 10. The P:V ratio grows with the synthesis time and reaches a plateau at a value of approximately 2:1 after 40 min. This value is entirely consistent with a number of XPS studies of VPO catalysts in which the Schofield sensitivity factors were applied. Studies which used internal standards tend to report lower surface P:V ratios [1].

4. Discussion

4.1. XPS characterisation

XPS is supposed to be one of the most informative techniques for determination of the surface chemical composi-

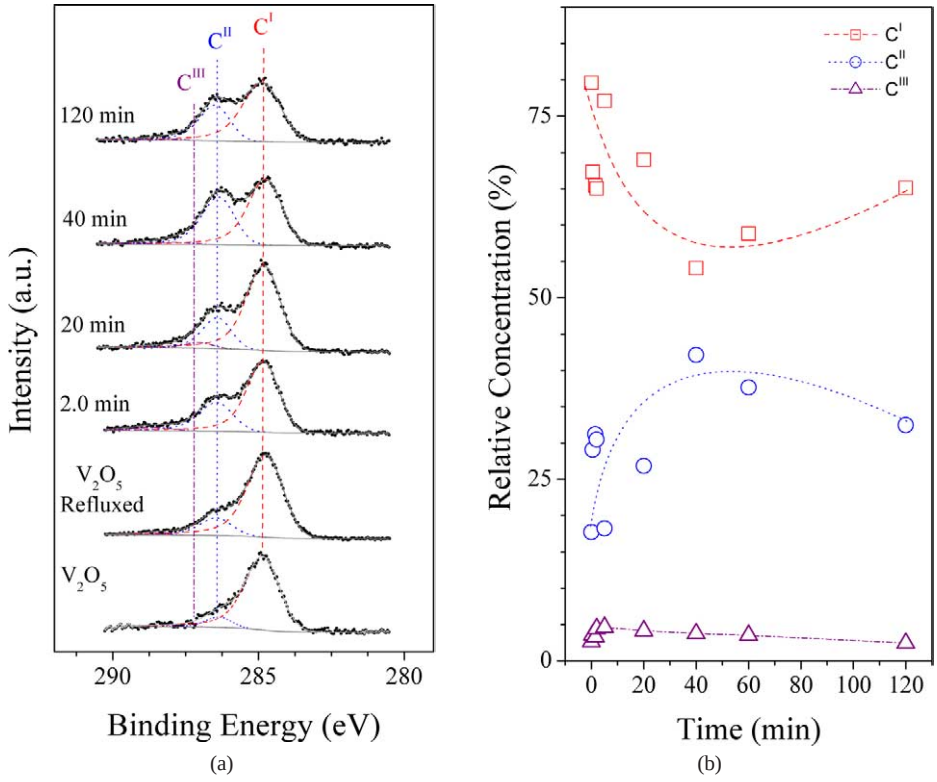

Fig. 9. (a) C 1s core-level spectra obtained from V_2O_5 and VPO samples recovered after specified time. (b) Relative concentration of the carbon species as a function of the synthesis time.

tion and the catalytically active sites in heterogeneous catalysis. The downside of the technique is the "ex situ" analysis and sensitivity to sample "nature": conductor (semiconductor) or insulator. However, if the ex situ XPS data are supplemented with the data of in situ techniques, really valuable information can be obtained. The XPS studies of nonconducting samples are associated with the "sample charging" problem. Thus, photo-emitted core-level electrons leave positive holes behind, which are neutralised by conducting electrons in the case of conducting or semiconducting samples. In the case of insulators, photoemission of core-level and secondary electrons causes an unevenly distributed positive charge. This phenomenon is referred to as a charge effect. The main problem associated with this effect is that photoelectron lines get broader losing resolution and/or shift toward high BE, thus hindering calibration. A number of the XPS studies of VPO catalysts found in the literature demonstrates the importance of this issue [20–26]. Coulston et al. [35] proposed the following equation for the definition of vanadium oxidation states, V_{ox},

$$V_{ox} = 13.82 - 0.68\big[\mathrm{BE(O\ 1s)} - \mathrm{BE(V\ 2p_{3/2})}\big], \qquad (1)$$

where BE(O 1s) and BE(V $2p_{3/2}$) are an average BE of the O 1s and V $2p_{3/2}$ lines. This equation overcomes calibration problems because the subtraction of BEs cancels a homogeneous BE shift. Eq. (1) also reflects an "initial state" effect. Electron transfer from vanadium to oxygen should result in a low BE shift of the O 1s line, whereas the V 2p lines should experience a high BE shift. So, the calculated oxidation state of vanadium increases. However, Eq. (1) is completely correct only for a single-component system. As demonstrated above (see, for instance, Figs. 4, 7, and 8), VPO samples are multicomponent systems. For instance, the ionic oxide-type oxygen characterised by the O 1s peak at 530.0 eV (O^I) is *gradually* replaced for the covalent phosphate oxygen characterised by the peak at 531.2 eV (O^{II}).

On the other hand, multicomponent analysis of the V 2p region is rather ambiguous if nonmonochromatic X-ray excitation were used. Thus, for the nonmonochromatic Mg-K_α radiation, the V $2p_{1/2}$ peak overlaps with the O 1s satellite due to Mg-$K_{\alpha_{3,4}}$ and the mathematic subtraction of the O 1s satellite is required before fitting can be applied to the V 2p region. The monochromatic Al-K_α radiation used for the present study avoids this problem. The V 2p region could be curve-fitted without preliminary satellite subtraction, which increases the reliability of the procedure.

As described under Results, the V 2p region was fitted with four doublets, which relate to four chemical states of vanadium, namely the oxygen defect (V^{3+}), $VOHPO_4 \cdot 0.5H_2O$ (V^{4+}), V_2O_5 (V^{5+}), and $VOPO_4 \cdot 2H_2O/VOPO_4 \cdot H_2O$ (V^{5+} hydrate). The vanadium and oxygen components assignment is summarised in Tables 1 and 2, respectively; the curve-fit analysis is consistent with the literature data as shown in Table 3. It should be stressed that the detailed analysis of the O 1s region is missed in the literature. The O 1s peak at 530.0 eV (O^I) has been related to an oxide species. This species was correlated with V_2O_5 since vana-

Table 3
XPS characteristics of the oxidation states of vanadium

Solid	BE (FWHM) (eV)		Δ(O 1s–V $2p_{3/2}$) (eV)	V_{ox}[a]	Energy reference[b] (eV)	Preparation	Reference
	V $2p_{3/2}$	O 1s					
$VOHPO_4 \cdot 0.5H_2O$	517.5 (2.0)	532.2 (3.0)	14.7	3.8	284.6	Organic	[25]
	517.2				284.6	Organic	[21]
	516.6	531.2	14.6	4.0	284.8	Organic	The present work
$(VO)_2P_2O_7$	517.3	531.8	14.5	4.0	285.0	Aqueous	[22]
	516.7 (2.0)	531.1 (2.4)	14.5	4.0	285.0	Solid-state reaction	[20]
	517.9	532.5	14.6	3.9	285.0	Organic	[23]
	517.3				284.6	Organic	[21]
β-$VOPO_4$	518.2 (1.6)	531.4 (2.0)		4.8	285.0	Solid-state reaction	[20]
	518.6	531.6	13.0	5.0	285.0	Aqueous	[22]
α-$VOPO_4$	516.6 (1.8)					Aqueous	[24]
α_{II}-$VOPO_4$	516.5 (1.7)	532.7 (2.2)	16.2	2.8	284.6	Organic	[25]
δ-$VOPO_4$	518.0	531.0	13.0	5.0	284.5	Organic	[26]
V_2O_5	517.6	530.6	13.0	5.0	284.8		[38]
	518.3				284.8		[39]
	517.4	530.6	13.2	4.8	284.8		[40]
	517.4				284.8		[22]
	517.4	530.3	12.9	5.0	284.8		[41]
	517.6				284.8		[42]
	517.3				284.8		[43]
	517.4	530.0	12.6	5.2	284.8		The present work
V_2O_3	516.8				284.8		[39]
$VOPO_4 \cdot 2H_2O$, $VOPO_4 \cdot H_2O$	518.1	531.2	13.1	5.0	284.8		The present work
Defects on V_2O_5	515.5	531.2	15.7	3.3	284.8		The present work

[a] The average oxidation state was calculated by using Eq. (1).
[b] The position of the C 1s peak.

dium oxide consuming during synthesis was accompanied by a decrease in intensity of the peak at 530.0 eV. The next O 1s peak at 531.2 eV (O^{II}) was identified as a phosphated oxygen species. The peak was observed to increase in intensity as synthesis time evolved, reflecting the formation of phosphate species. Two O 1s peaks were also identified at 531.9 eV (O^{III}) and 532.9 eV (O^{IV}) and were assigned as OH and H_2O, respectively. The water concentration increases to almost 30 at% by 5 min of synthesis (Fig. 8, see the peak at 532.8 eV, the O^{IV} state) and showed a very modest decrease. In fact, water is the product of vanadium reduction in alcohol media; therefore some accumulation of H_2O in sample porosity is expected. The other possible source of water is the disproportionation of the alcohol hydroxyl groups in vacuum.

It should be noted that carbon contamination was a factor that greatly hindered the quantitative analysis. The carbon contamination was as high as 40 at% for the refluxed V_2O_5 samples dropping down to 16 at% in 120 min. The problem is that a decrease of total carbon percentage is accompanied by the growth of the amount of the partially oxidised carbon represented by the C 1s peak at 286.4 eV as shown Fig. 9. The oxygen species bond to carbon might result in the O 1s signal in the range from 530.5 to 531.5 eV. Also, carbon might attach to the ionic oxygen, V=O bond, transforming this species into a more covalent one. As shown Fig. 7, according to the intensity of the V $2p_{3/2}$ component at 517.4 eV, the hydrate-rich sample contains an essential amount of V_2O_5, whereas the ionic oxygen is almost absent in the O 1s spectra. This phenomenon cannot be explained by simply losing resolution and broadening of the V 2p lines because (i) other XPS lines in particularly C 1s did not get broader and (ii) the V_2O_5 reflections are clearly detected by XRD (Fig. 6). On the other hand, by assuming that the transformation of the ionic oxygen may be due to the C–O bond formation and therefore the O 1s peak shifts to 531.2 eV, a good qualitative and quantitative agreement between the vanadium and oxygen species can be achieved.

A preliminary summary of the XPS results conclude that the ex situ XPS data showed a qualitative correlation with in situ XRD, whereas quantitative analysis required taking into account several factors.

4.2. Chemical mechanism: From V_2O_5 to $VOHPO_4 \cdot 0.5H_2O$

This study of the crystallisation of $VOHPO_4 \cdot 0.5H_2O$ has successfully identified $VOPO_4 \cdot 2H_2O$ and $VOPO_4 \cdot H_2O$ by XPS and XRD as a phase, which forms at short synthesis times. The preponderance of the V $2p_{3/2}$ peak at 518.2 eV in the hydrate-rich phase (see Figs. 6 and 7) and the occurrence of a peak at this binding energy are observed in samples isolated from the synthesis mixture at short synthesis times after the addition of *ortho*-H_3PO_4. A further point of interest is

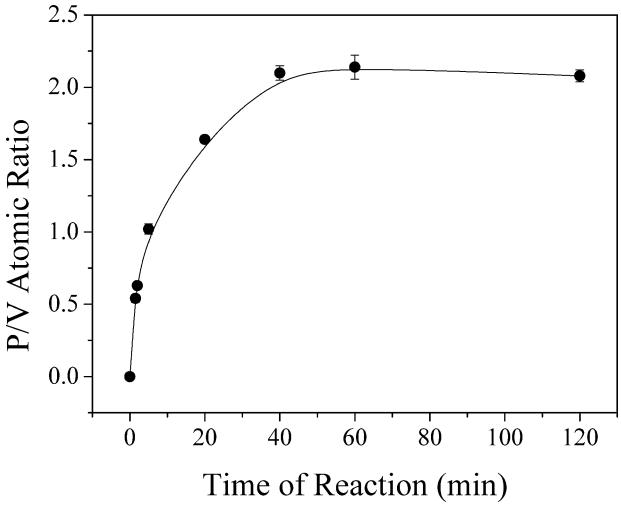

Fig. 10. P:V ratio calculated from XPS data as a function of the synthesis time.

the similarity in phase evolution during in situ monitoring of the synthesis by XRD (see Fig. 1) and the ex situ analysis by XPS (see Fig. 5).

In all major features, the XPS data support the earlier proposed mechanism [19], namely that $VOPO_4 \cdot 2H_2O$ dehydrates to $VOPO_4 \cdot H_2O$, delaminates to relieve strain, and the delaminated edges of $VOPO_4 \cdot H_2O$ serve as the nucleation points for growth of $VOHPO_4 \cdot 0.5H_2O$ as well as reductions of $VOPO_4 \cdot H_2O$ phase. The additional insight provided by the XPS technique allows us to trace the development of surface vanadium, oxygen and carbon states as well as the surface P:V ratio.

The evolution of vanadium and oxygen surface states is entirely self-consistent. The carbon states, particularly the development of partially oxidised carbon-containing species, are not surprising since reduction of V^{5+} by alcohol will inevitably lead to oxidation of the alcohol. A point of interest is the retention of the oxidised carbon species on the surface, although it must be pointed out that there is no evidence from XRD *d* spacings for $VOPO_4 \cdot 2H_2O$, $VOPO_4 \cdot H_2O$, or $VOHPO_4 \cdot 0.5H_2O$ for any appreciable intercalation of carbon-containing species when synthesis is performed at reflux. As noted above, carbon contamination was high for all samples but decreases from 40 at% at short synthesis times to 16 at% after 120 min. In view of the nature of the crystalline habit of the $VOHPO_4 \cdot 0.5H_2O$ particles which form, namely distorted platelets with a preponderance of exposed (001) planes, we may postulate that partially oxidised carbon species attached to the {001} facets of $VOHPO_4 \cdot 0.5H_2O$ may disrupt growth on this face, favouring addition of vanadium to the side faces giving the well-known platelet-like habits.

A further feature of interest is the evolution of the P:V surface ratio (see Fig. 10). The V_2O_5 component added to the alcohol mixture never fully dissolves during reflux prior to phosphorus addition. This is evident in Figs. 1 and 2, which show some undissolved vanadium oxide present. Approximately 60–70% of the initial charge of V_2O_5 remains undissolved after 4 h of reflux, prior to the addition of *ortho*-H_3PO_4. The maximum surface P:V ratio corresponds to the time at which the V^{4+} species (Fig. 5), the O^{II} species (Fig. 8), and the C^{II} species (Fig. 9) all approach their maximum values. The increasing P:V ratio observed up to 40 min may be largely assigned to rapid dissolution of V_2O_5 and formation of a VPO phase following phosphate addition. The cross sections (Fig. 3) show individual particles that appear to delaminate and evolve well beyond the time when all $VOPO_4 \cdot H_2O$ has been transformed with a densification of the interior of these particles at larger synthesis times. This mechanism of $VOHPO_4 \cdot 0.5H_2O$ formation is entirely consistent with the work of Okuhara's group [36,37]. This group prepared $VOPO_4 \cdot 2H_2O$ separately and added 2-methylpropan-1-ol at two temperatures. They observed exfoliations of the platelets caused by intercalation of alcohol molecules. Our mechanism, for higher synthesis temperatures, also identified $VOPO_4 \cdot 2H_2O$ formation and delamination, followed by growth of $VOHPO_4 \cdot 0.5H_2O$ and densification as important steps in the synthesis. Important evidence in this regard is the increase in particle volume of 20 μm^3 in Fig. 2 to a value of over 900 μm^3 in Fig. 3.

5. Summary

It is apparent from this study that it is possible to follow the mechanism of crystal growth by XPS. This study demonstrates the importance of monochromatic X-ray source used for the detailed characterisation of the surface species formed during the $VOHPO_4 \cdot 0.5H_2O$ synthesis.

Remarkably in situ monitoring of the synthesis by XRD and the ex situ analysis by XPS demonstrate very consistent results. The additional insight provided by the XPS technique allows us to trace the development of surface vanadium, oxygen, and carbon states as well as the surface P:V ratio. $VOPO_4 \cdot 2H_2O$ and $VOPO_4 \cdot H_2O$ were successfully identified by XPS as a phase, which forms at short synthesis times. The occurrence of the V $2p_{3/2}$ peak at 518.1 eV was observed in samples recovered from the synthesis mixture at short synthesis times after the addition of *ortho*-H_3PO_4. The XPS data point to a palpable trend whereby the hydrate phase concentration decreases whereas the V $2p_{3/2}$ peak at 516.6 eV characterised $VOHPO_4 \cdot 0.5H_2O$ increases in intensity. A consistent decrease in intensity of XRD reflections of V_2O_5 and depleting V $2p_{3/2}$ peak at 517.4 eV represent the consumption of V_2O_5 in the reaction. All XPS data were in a good agreement with the earlier proposed mechanism [19], which supposed that $VOPO_4 \cdot 2H_2O$ dehydrates to $VOPO_4 \cdot H_2O$ and delaminates and the delaminated edges of $VOPO_4 \cdot H_2O$ serve as the nucleation point for growth of $VOHPO_4 \cdot 0.5H_2O$.

Acknowledgment

D.Z. acknowledges the Foundation of the University of Limerick for support in the form of a Research Scholar.

References

[1] B.K. Hodnett, Heterogeneous Catalytic Oxidation: Fundamentals and Technological Aspects of the Selective and Total Oxidation of Organic Compunds, Wiley, New York, 2000.
[2] E. Bordes, Catal. Today 1 (1987) 499.
[3] G. Centi, F. Trifiro, J.R. Ebner, V.M. Franchetti, Chem. Rev. 88 (1988) 55.
[4] G. Centi, Catal. Today 16 (1993) 5.
[5] G. Centi, Catal. Today 16 (1993) 1.
[6] V.V. Guliants, J.B. Benziger, S. Sundaresan, I.E. Wachs, J.-M. Jehng, J.E. Roberts, Catal. Today 28 (1996) 275.
[7] J.R. Ebner, M.R. Thompson, Catal. Today 16 (1993) 51.
[8] G.J. Hutchings, A. Desmartin-Chomel, R. Olier, J.C. Volta, Nature 368 (1994) 41.
[9] G.J. Hutchings, A. Burrows, S. Sajip, C.J. Kiely, K.E. Bere, J.C. Volta, A. Tuel, M. Abon, in: Understanding the Microstructural Transformation Mechanism which Takes Place during the Activation of Vanadium Phosphorus Oxide Catalyst, 3rd World Congress on Oxidation Catal., San Diego, CA, Elsevier Science, 1997, p. 209.
[10] G.J. Hutchings, C.J. Kiely, M.T. Sananes-Schulz, A. Burrows, J.C. Volta, Catal. Today 40 (1998) 273.
[11] H.S. Horowitz, C.M. Blackstone, A.W. Sleight, G. Teufer, Appl. Catal. 38 (1988) 193.
[12] D.J. Thompson, M.O. Fanning, B.K. Hodnett, J. Mol. Catal. A: Chem. 198 (2003) 125.
[13] B.K. Hodnett, Catal. Rev.-Sci. Eng. 27 (1985) 373.
[14] J.W. Johnson, D.C. Johnston, A.J. Jacobson, J.F. Brody, J. Am. Chem. Soc. 106 (1984) 8123.
[15] E.A. Lombardo, C.A. Sanchez, L.M. Cornaglia, Catal. Today 15 (1992) 407.
[16] G. Centi, F. Trifiro, G. Poli, Appl. Catal. 19 (1985) 225.
[17] M. Abon, J.-C. Volta, Appl. Catal. A 157 (1997) 173.
[18] C.J. Kiely, A. Burrows, S. Sajip, G.J. Hutchings, M.T. Sananes, A. Tuel, J.-C. Volta, J. Catal. 162 (1996) 31.
[19] L. O'Mahony, J. Henry, D. Sutton, T. Curtin, B.K. Hodnett, Appl. Catal. A 253 (2003) 409.
[20] T.P. Moser, G.L. Schrader, J. Catal. 104 (1987) 99.
[21] A. Satsuma, A. Hattori, A. Furuta, A. Miyamoto, T. Hattori, Y. Murakami, J. Phys. Chem. B 92 (1988) 2275.
[22] G.C. Bond, S. Flamerz, Appl. Catal. 46 (1989) 89.
[23] N. Harrouch Batis, H. Batis, A. Ghorbel, J.C. Vedrine, J.C. Volta, J. Catal. 128 (1991) 248.
[24] Y. Zhang, R.P.A. Sneeden, J.C. Volta, Catal. Today 16 (1993) 39.
[25] L.M. Cornaglia, E.A. Lombardo, Appl. Catal. A 127 (1995) 125.
[26] P. Delichere, K.E. Bere, M. Abon, Appl. Catal. A 172 (1998) 295.
[27] S.M. Clark, Nucl. Instrum. Methods Phys. Res. A 381 (1996) 161.
[28] S.M. Clark, R.J. Cernik, A. Grant, S. York, P.A. Atkinson, A. Gallagher, D.G. Stokes, S.R. Gregory, N. Harris, W. Smith, M. Hancock, M.C. Miller, K. Ackroyd, R. Farrow, R. Frances, in: A New White Beam Powder Diffraction Facility at the Daresbury Laboratory Synchrotron Radiation Source, Materials Science Forum: Fourth European Powder Diffraction Conference EPDIC IV, Switzerland, Transtec Publications, 1996, p. 213.
[29] P. Barnes, A.C. Jupe, S.L. Colston, S.D. Jacques, A. Grant, T. Rathbone, M. Miller, S.M. Clark, R.J. Cernik, Nucl. Instrum. Methods Phys. Res. B 134 (1998) 310.
[30] D.A. Shirley, Phys. Rev. 55 (1972).
[31] J.H. Scofield, J. Electron Spectrosc. Relat. Phenom. 8 (1976) 129.
[32] S. Doniach, M. Sunjic, J. Phys. 4C31 (1970) 285.
[33] N. Fairley, CasaXPS, Neal Fairley, 1999–2002.
[34] E. Bordes, P. Courtine, J.W. Johnson, J. Solid State Chem. 55 (1984) 270.
[35] G.W. Coulston, E.A. Thompson, N. Herron, J. Catal. 163 (1996) 122.
[36] Y. Kamiya, S. Ueki, N. Hiyoshi, N. Yamamoto, T. Okuhara, Catal. Today 78 (2003) 281.
[37] N. Yamamoto, N. Hiyoshi, T. Okuhara, Chem. Mater. 14 (2002) 3882.
[38] G. Bliznakov, Y. Pesheva, D. Klissurski, M. Marinov, V. Kozhukharov, Appl. Catal. 29 (1987) 211.
[39] N.K. Nag, F.E. Massoth, J. Catal. 124 (1990) 127.
[40] P. Mezentzeff, Y. Lifshitz, J.W. Rabalais, Nucl. Instrum. Methods Phys. Res. B 44 (1990) 296.
[41] A. Meisel, K.H. Hallmeier, R. Szargan, J. Muller, W. Schneider, Phys. Scripta 41 (1990) 513.
[42] J. Soria, J.C. Conesa, M.L. Granados, R. Mariscal, J.L.G. Fierro, J. Catal. 120 (1989) 457.
[43] J.L.G. Fierro, L.A. Arrua, J.M.L. Nieto, G. Kremenic, Appl. Catal. 37 (1988) 323.